Title

Probing demyelination and remyelination of the cuprizone mouse model using multimodality MRI

Journal

Journal of Magnetic Resonance Imaging, 50(6)

ISSN

1053-1807

Authors

Wang, Nian
Zhuang, Jie
Wei, Hongjiang
et al.

Publication Date

2019-12-01

DOI

10.1002/jmri.26758

Peer reviewed

HHS Public Access

Author manuscript

J Magn Reson Imaging. Author manuscript; available in PMC 2020 December 01.

Published in final edited form as:

J Magn Reson Imaging. 2019 December ; 50(6): 1852–1865. doi:10.1002/jmri.26758.

Probing demyelination and remyelination of cuprizone mice model using multimodality MRI

Nian Wang, PhD[1,2], **Jie Zhuang, PhD**[2], **Hongjiang Wie, PhD**[2], **Russell Dibb, PhD**[1], **Yi Qi, MD**[1], **Chunlei Liu, PhD**[3,4]

[1]Center for In Vivo Microscopy, Duke University, Durham, North Carolina, USA

[2]Brain Imaging and Analysis Center, Duke University, Durham, North Carolina, USA

[3]Department of Electrical Engineering and Computer Sciences, University of California, Berkeley, CA, USA

[4]Helen Wills Neuroscience Institute, University of California, Berkeley, CA, USA

Abstract

Background: Various studies by MRI exhibit that corpus callosum (CC) is most vulnerable to cuprizone administration, detecting demyelination and remyelination process using different MRI parameters are however lacking.

Purpose: To investigate the sensitivity of multiparametric MRI both in vivo and ex vivo for demyelination and remyelination.

Study Type: Prospective.

Animal Model: Cuprizone mice model with age matched control group (n=5), 4-week cuprizone exposure group followed by 9-week on a normal diet (n=6), and a 13-week cuprizone exposure group (n=6).

Field Strength/Sequence: 3D GRE, T2-weighted and diffusion tensor imaging (DTI) at 7.0 T and 9.4 T.

Assessment: Quantification of DTI metrics, quantitative susceptibility mapping (QSM), and T2-weighted imaging intensity in major white matter bundles.

Statistical Tests: Non-parametric permutation tests were used with cluster-forming threshold as 3.09 (equivalent to $p = 0.001$), and the significant level as $p = 0.05$ with Family-wise (FWE) correction.

Results: In vivo susceptibility values increased from −11.7 to −0.7 ppb ($p < 0.001$) in CC and from −13.7 to −5.1 ppb ($p < 0.001$) in Anterior commissure (AC) after 13-week cuprizone exposure. Ex vivo susceptibility values increased from −25.4 to 7.4 ppb ($p < 0.001$) in CC and from −41.6 to −15.8 ppb ($p < 0.001$) in AC. Susceptibility values showed high variations to demyelination for in vivo studies (94.0% in CC, 62.8% in AC). Susceptibility values exhibited

Correspondence Address: Chunlei Liu, Ph.D., Department of Electrical Engineering and Computer Sciences, Helen Wills Neuroscience Institute at the University of California, Berkeley. 505 Cory Hall, Berkeley, CA 94720, USA. Phone: (510)664 7596, chunlei.liu@berkeley.edu.

higher variations than radial diffusivity for ex vivo studies (129.1% vs 28.3% in CC, 62.0% vs 25.0% in AC). In addition to the differential susceptibility variations in different white matter tracts, intraregional demyelination variation was also present not only in CC but also in AC area by voxel-based analysis.

Data Conclusion: QSM is sensitivity to demyelination process of cuprizone exposure, which can be a complementary technique to conventional T2-weighted images and DTI metrics.

Keywords

Quantitative susceptibility mapping (QSM); Cuprizone; Demyelination; Remyelination; Multiple Sclerosis (MS); Diffusion Tensor Imaging (DTI)

Introduction

Multiple sclerosis (MS) is an autoimmune disease characterized by demyelination and inflammation of the central nervous system (CNS) in both white and gray matters. The exact mechanism of MS development and progression remains to be elucidated (1,2). Animal models, including the cuprizone mouse model, have greatly enhanced the knowledge of MS pathophysiology and afford the opportunity to investigate the demyelination and remyelination process (3). The cuprizone model does not model the full disease process of MS, continued exposure of the copper chelator cuprizone results in a white matter (WM) pathology that is similar to pattern III MS lesions, accompanied by extensive macrophage/microglia activation, oligodendrocytes apoptosis, and demyelination (2).

By employing diffusion tensor imaging (DTI) to quantify abnormalities in the WM fiber tracts of cuprizone model, it has been reported that axial diffusivity (AD) and radial diffusivity (RD) were significantly higher in both the corpus callosum and external capsule of the cuprizone-fed mice when compared with controls (4). Recent results from the cuprizone model using magnetization transfer imaging (MTI) showed that demyelination was not limited to the midsagittal line of the corpus callosum (CC), and also occurred in the lateral and medial CC (5). Guglielmetti et al. reported that both T2 and magnetization transfer ratio (MTR) measures are highly correlated to the brain microstructure and underlying histopathological events following cuprizone administration (6). Furthermore, diffusion kurtosis imaging (DKI) was found to be sensitive to alterations of both corpus callosum areas and cortical areas, which is complementary to DTI metrics for the characterization of demyelination in both WM and gray matter (GM) (7).

Quantitative susceptibility mapping (QSM) has been developed to solve the ill-posed phase-to-susceptibility inverse problem and derive the voxel-based magnetic susceptibility (8). The susceptibility tensor imaging (STI), requiring phase images at different subject orientations with respect to the main magnetic field, has been proposed to better understand the magnetic susceptibility anisotropy (MSA) and to study white matter microstructures (9,10). QSM may be more sensitive and specific to dysmyelination process than diffusion metrics (11,12). Susceptibility contrast between GM and WM is significantly diminished in the shiverer mice compared to the control mice (11). The loss of susceptibility contrast is due to the absence of functional myelin surrounding axons within the WM of the shiverer mice. Whereas,

fractional anisotropy (FA) were reduced by less than 20% in the shiverer mice, which may suggest that the change of susceptibility values is more sensitive to myelin itself.

Although various MRI parameters have been used as imaging biomarkers to probe the demyelination process, the sensitivity to demyelination is likely to be dependent on different parameters. The majority of cuprizone mice model studies mainly focused on the CC region (4,5,13), while demyelination/remyelination studies of major WM tracts in the whole brain are still lacking (14). Furthermore, most QSM studies were performed in postmortem mouse brains (10,11,14). Ex vivo studies provide superior imaging quality allowing higher imaging resolution and the absence of motion artifacts, while in vivo MRI measurements can reflect the structural properties of the tissue in vivo but often suffer from lower imaging resolution and subject motion (15). It has been shown that fixation can alter the ratio of intracellular and extracellular spaces and membrane permeability (15), thus whether in vivo and ex vivo QSM are comparable in detecting WM pathology is still unknown.

Materials and Methods

Animal Model

All animal studies were approved by the local Institutional Animal Care and Use Committee (IACUC). Male C57/BL6J mice (n = 17, 8 weeks old at baseline, Jackson Laboratory, Bar Harbor, ME) were separated into three diet groups: the cuprizone-fed group (DEMY group, n=6) received diet of chow mixed with 0.2% cuprizone diet (Sigma Aldrich, St. Louis, MO) over the course of 13 weeks to induce a chronic state of CNS demyelination; the recovery group (REMY group, n=6) received 0.2% cuprizone diet for 4 weeks, followed by 9 weeks of recovery time with normal diet of chow; the control group (CTRL group, n=5) received normal diet of chow for 13 weeks. Animals from each diet group were sacrificed after in-vivo MRI imaging. Brains were perfused using a transcardial access with a mixture of 0.9% saline and gadolinium (Gd) contrast agent (10:1, v:v) (Bracco Diagnostics, Princeton, NJ) (12). Five specimens in each group were immersed in buffered formalin for 24 hours and then moved to a 1:200 solution of Gd/saline for about 3 weeks to shorten T1 and reduce scan time. One specimen in DEMY and REMY group was perfused without Gd contrast agent to estimate the influence of the contrast agent used for the ex vivo MRI studies.

In vivo MRI protocol

In vivo MRI was performed on a 20-cm-bore 7 T magnet (Bruker BioSpec 70/20 USR, Billerica, MA) interfaced to an Avance III system. The scanner was equipped with shielded gradients (440 mT/m amplitude) providing integrated fieldmap shims up to the second order. A high-sensitivity cryogenic radiofrequency (RF) surface coil was used for transmission and reception (Bruker CryoProbe). A 3D printer (Stratasys Dimension, Eden Prairie, MN) was used to make custom parts for the nose cone and for proper positioning of the animal inside a cryogenic surface coil. Five mice in each group were anesthetized using 5% isoflurane in O_2/N_2O (ratio 21% / 79%) and maintained at 1.5% isoflurane in O_2/N_2O. Respiration (about 80 ± 15 breaths/min) and external body temperature were monitored during imaging using an MR-compatible small animal monitoring and gating system (SA Instruments, Stony

Brook, NY, USA). External body temperature was maintained at 37 ºC with a heating circulator bath (Thermo Scientific Haake, Karlsruhe, Germany).

A 3D multi-echo gradient echo pulse sequence (MGE) was acquired with field of view (FOV) of (19.2 × 14.4 × 9.6) mm^3 and 100 μm isotropic spatial resolution with even echoes flow compensation. The acquisition parameters of the MGE sequence were: TR = 250 ms, TE =3.7 ms, echo spacing = 5.5 ms, 10 echoes, BW = 125 kHz, flip angle = 30º, 1 average, and scan time = 90 minutes with gating. The readout direction is along the main magnetic field.

T2-weighted images were acquired using a rapid acquisition with refocused echoes (RARE) sequence. The acquisition parameters were: effective TE = 45 ms, TR = 4000 ms, RARE factor = 8, bandwidth = 62.5 kHz, 8 averages, FOV of 18 cm × 18 cm, 150 μm × 150 μm spatial resolution with 14 slices, slice thickness = 300 μm, scan time = 8 minutes. The readout direction is along the main magnetic field.

Ex vivo MRI protocol

Fixed specimens were scanned at 9.4 T (Oxford 8.9-cm vertical bore; Agilent VnmrJ 4.0 imaging console) using a multi-echo, 3D gradient echo sequence. The shielded coils provide gradients of up to 2000 mT/m amplitude. Each specimen was fitted in an acrylic holder filled with fomblin (Ausimont USA, Inc., Thorofare, NJ, USA) to limit susceptibility artifacts at the surface of the tissue. The acrylic specimen holder was placed in a homemade solenoid radiofrequency coil with manual shimming up to the 2^{nd} order. The scan parameters were as follows: matrix size = 512 × 256 × 256, FOV = (22 × 11 × 11) mm^3, flip angle = 65º, TE = 1.9 ms, echo spacing = 3.1 ms, 12 echoes, BW = 125 kHz, and TR = 100 ms. The spatial resolution was 43 μm isotropic and the scan time was about 120 minutes.

DTI were acquired using a diffusion-weighted 3D spin-echo sequence (19) with the FOV of (22 × 11 × 11) mm^3 and matrix size of 256 × 128 × 128. The other parameters were as follows: TE = 25 ms, and TR = 200 ms. One image volume was acquired without diffusion weighting. Twelve diffusion-encoding directions were used at a b-value of 1700 s/mm^2 to allow the calculation of diffusion tensor. The gradient separation time was 7 ms, the diffusion gradient duration time was 4 ms, and the gradient amplitude was ~ 90 G/cm. Total scan time for DTI was about 12 hours. Temperature was monitored throughout the scans (~ 25 ºC) and fluctuation was recorded to be below 1 ºC.

Imaging Analysis

QSM Reconstruction—The phase data from the GRE acquisition was used to reconstruct QSM images using STI Suite (University of California, Berkeley) (16). Specifically, the phase of the raw data was unwrapped using a Laplacian-based phase unwrapping method (8). The background phase was removed using the V-SHARP method with kernel size up to 25 (17). Magnetic susceptibility was then obtained from the local tissue phase by solving an inverse problem using the improved LSQR (iLSQR) method (16,18):

$$f(r) = FT^{-1}\left\{\left(\frac{1}{3} - \frac{k_z^2}{k^2}\right)\chi(k)\right\}\gamma B_0$$

where FT^{-1} is the inverse Fourier transform, $\chi(k)$is the susceptibility map in the frequency domain, $k$is the reciprocal space vector and k_z is its z-component, $\gamma$is the gyromagnetic ratio for water proton, $B_0$is the magnitude of the main magnetic field.

DTI Reconstruction—The diffusion tensor was calculated at each voxel and used to generate various tensor derived scalar images including fractional anisotropy (FA), eigenvalues, eigenvectors, and mean diffusivity (MD) maps (19,20). Axial diffusivity (AD) and radial diffusivity (RD) were also derived using Matlab (The MathWorks, Natick, MA, USA) based on Diffusion Toolkit software (21).

Image Registration—Images were co-registered using a two-step process. Briefly, magnitude images from each animal were linearly registered to a standard-space template in the Waxholm Space (22) using FMRIB's linear image registration tool (FLIRT) (Oxford University, UK). A nonlinear registration was then applied using FSL's nonlinear registration tool, FNIRT (Oxford University, UK). The transformation matrixes were then applied to in vivo QSM and ex vivo QSM and DTI metrics for voxel-based analysis. Reverse transformation of the Waxholm Space into each subject's native space was performed using the inverse transformation matrixes for ROI-based analysis. For the regional QSM heterogeneity study in the same WM bundle (anterior commissure), ROIs were manually segmented according to the previous references (5,13). The accuracy of the transformation was inspected for each map using the ITK-SNAP software with landmarks manually placed in CC and AC regions (Supplemental Fig. 1) (23). The maximum registration error was 2 pixels as evaluated by two independent raters.

Figure 1 illustrates the delineation of anterior commissure (green), corpus callosum (blue), and hippocampus commissure (red) in the native space of one mouse brain GRE magnitude image, the genu (gCC), body/isthmus (iCC), and splenium (sCC) were pointed by white arrows. The anterior commissure was further subdivided to 3 parts: anterior part (AAC), intermediate part (IAC), and posterior part (PAC), in order to investigate the intraregional heterogeneity of demyelination and remyelination process.

In vivo T2-weighted images were normalized to the mean CSF signal in the third ventricle. The variation of different MRI metrics between CTRL group and DEMY group is calculated as:

$$\text{Variation} = \left(M_{\text{CTRL}} - M_{\text{DEMY}}\right)/M_{\text{CTRL}}$$

Where M stands for the mean T2-weighed signal, diffusion metrics, or QSM values of CTRL group (M_{CTRL}) or DEMY group (M_{DEMY}). All the MRI images were evaluated by two independent raters.

Histological analysis—Histological examinations were performed after the ex vivo MRI scans. Coronal 6-μm thick slices were stained with myelin staining agent (LFB – Luxol Fast Blue) and iron staining agent (PPB – Perl's Prussian Blue). As a control for iron staining, one slice of human liver tissue was also stained with PPB with the same protocol simultaneously. Slides were imaged using Axioscop2 FSmot optical microscope with EC PlanNeofluar Zeiss lens at 10x magnification, 0.3 aperture under the same settings and light conditions. The histological slices were evaluated by two pathologists with more than 5 years of experience.

Statistics—Direct comparisons between CTRL and DEMY, between CTRL and REMY were performed using the Statistical nonParametric Mapping (SnPM13) installed in SPM 12, (Wellcome Institute of Cognitive Neurology, London, UK), under MATLAB (Mathworks Inc., Natick, MA, USA) (24). Due to the small number of mice in each group (n = 5), non-parametric permutation tests were used with 5000 permutations for voxel-based analysis. Cluster-forming threshold was set as 3.09 which is equivalent to $p = 0.001$, and the significance level was set as $p = 0.05$ with Family-wise (FWE) correction. Variance smoothing = 2 mm x 2 mm x 2 mm. Clusters above this threshold were identified as significant and reported in the result section.

Results

Cuprizone diet

Throughout the duration of the experiment all mice fed with cuprizone appeared clinically normal and did not display symptoms such as ataxia, seizures, or anorexia. The mean body weight of DEMY, REMY, and CTRL groups were 25.2 ± 0.8 g, 29.4 ± 2.3 g, 31.4 ± 1.1 g, individually. There was no statistically significant body weight variation between REMY group and CTRL group ($p = 0.092$), while significant body weight change was observed between DEMY group and CTRL group ($p < 0.001$), and between DEMY group and REMY group ($p < 0.001$). The brain volumes of DEMY, REMY, and CTRL groups were 459.6 ± 14.7 mm^3, 467.7 ± 16.6 mm^3, and 474.6 ± 12.9 mm^3 (Supplemental Fig. 2). The maximum volume difference among different groups was found between DEMY group and CTRL group (~ 4%) without a significant difference ($p = 0.161$).

T2-weighted images in vivo

Figure 2 shows the normalized T2-weighted images (a-c) of three groups (DEMY, REMY, and CTRL). T2-weighted images in CC area (white arrows) showed hyperintense signal (brighter) in DEMY group, while hypointense signal (darker) was found in REMY and CTRL group. Normalized T2-weighted images illustrated significant differences in signal intensity among three groups in the CC ($p < 0.001$ between DEMY and REMY, $p < 0.001$ between DEMY and CTRL, and $p = 0.024$ between REMY and CTRL) and AC ($p = 0.010$ between DEMY and REMY, $p = 0.012$ between DEMY and CTRL) areas, while no significant differences in HC area (black arrows, $p > 0.05$).

Region-specific QSM of different WM bundles in vivo

A representative set of in vivo susceptibility maps for the three groups are shown in Fig. 3a–3f. The three white matter bundles (CC, AC, and HC) exhibited the strongest diamagnetic susceptibility in CTRL group and the least diamagnetic susceptibility in DEMY group except the HC area, where there was no visual susceptibility difference among these three groups. The CC region appeared hypointense signal (more diamagnetic than surrounding GM) in CTRL group and REMY group. This hypointense appearance became barely visible in DEMY group with no apparent contrast distinction between CC and surrounding GM. The similar phenomenon was found in AC region, however, the AC in DEMY group exhibited slight darker than the surrounding GM. Compared to CTRL mice, these values represented an increase of magnetic susceptibility by 94.0 % of DEMY group ($p < 0.001$) and 51.3 % of REMY group ($p < 0.001$) in CC; by 62.8 % of DEMY group ($p < 0.001$) and 26.3 % of REMY group ($p = 0.015$) in the AC; while no significant differences were found in HC between CTRL group and DEMY group ($p = 0.218$), between CTRL group and REMY group ($p = 0.352$) (Fig. 4).

Region-specific QSM of different WM bundles ex vivo

A representative set of ex vivo susceptibility maps for the three different groups are also shown in Fig. 3g–3l). Two features could be identified from these images. First, the CC region exhibited hypointense appearance in both CTRL and REMY group, which was similar to the in vivo results. This hypointense appearance became hyperintense in DEMY group, which indicated an elevation of susceptibility values (brighter in QSM, black arrows). Second, compared to the CTRL mice, magnetic susceptibility values increased by more than 100.0 % of DEMY group (−25.4 vs 7.4 ppb) and 50.0 % of REMY group (−25.4 vs −12.7 ppb) in CC area; by 62.0 % of DEMY group (−41.6 vs −15.8 ppb) and 25.7 % of REMY group (−41.6 vs −30.9 ppb) in AC area (Fig. 4); while no significant differences were found in HC area between CTRL group and DEMY group ($p = 0.305$), between CTRL group and REMY group ($p = 0.254$). It was also interesting to note that the variation of susceptibility value was not only regionally different in different WM bundles, but also regional heterogeneous in the same WM bundle. For example, the anterior part of AC exhibited more paramagnetic susceptibility (brighter in QSM, white arrows) than the posterior part of AC.

Region-specific DTI parameters ex vivo

No visual distinction was identified on the FA maps for all three ROIs among the DEMY, REMY, and CTRL group (Fig. 5). Although both CC and AC showed dramatic susceptibility variations among these three groups, the FA maps of DEMY group and REMY group showed a strong contrast between GM and WM, similar to the CTRL group. The average FA values (mean ± standard deviation) of DEMY, REMY, and CTRL groups were 0.41 ± 0.05, 0.42 ± 0.07, and 0.44 ± 0.05 in CC area; 0.52 ± 0.03, 0.53 ± 0.04, and 0.54 ± 0.05 in AC area; 0.48 ± 0.04, 0.49 ± 0.04, and 0.51 ± 0.05 in HC area, respectively (Table 3).

Similarly, no significant differences were found between REMY group and CTRL group in CC by MD ($p = 0.378$), AD ($p = 0.165$), and RD ($p = 0.284$), while significant differences were found between DEMY group and CTRL group by MD ($p = 0.047$), AD ($p = 0.029$), and RD ($p = 0.014$). Compared to CTRL group, RD, AD and MD of DEMY group increased

28.3 %, 17.5%, and 22.2 % in CC, 25.0 %, 15.8 %, and 20.8 % in AC, respectively (Fig 6). No significant differences were found in HC between DEMY group and CTRL group ($p > 0.05$).

Intraregional heterogeneous QSM of major WM bundles

Figure 7 shows in vivo and ex vivo voxel-based analysis of QSM in CC, external capsule (EC), and cortex (CX) regions. CC structure was separated into genu (gCC), body/isthmus (iCC), and splenium (sCC) regions. Compared to CTRL group, the susceptibility values of DEMY group increased significantly in CC, EC (red arrows), and CX (blue arrows) areas. The variations were largely eliminated in REMY group; however, the significant susceptibility differences can be resolved in these regions between REMY and CTRL. Note the CX susceptibility variation was more extensive in the ex vivo results (h), but it was not as wide spread in the in vivo results (f).

To investigate the intraregional heterogeneity of AC region, in vivo and ex vivo regional susceptibility changes are illustrated in Figure 8. For the voxel-based susceptibility value analysis, significant differences ($p < 0.001$) were found in AAC, PAC, and IAC after 13 weeks of cuprizone administration (c), while there was no significant difference ($p > 0.05$) found in the PAC area between REMY and CTRL group (d). For the ROI-based analysis (e-f), the susceptibility value of DEMY group increased significantly compared to CTRL group ($p < 0.001$). Susceptibility value of REMY group also increased compared to CTRL group in the AC region ($p = 0.003$ for in vivo, $p = 0.006$ for ex vivo) except the PAC region. The in vivo PAC results were not shown due to the strong susceptibility source nearby the PAC region (a and b, black arrowheads). The susceptibility values of three groups remained negative in all AC sub-regions except for the AAC region of DEMY group (Table 2). The intraregional variations of AC also exhibited by DTI metrics of MD, AD, and RD, however, not by FA (Supplemental Fig. 3).

Influence of Gd contrast agent for ex vivo QSM

Figure 9 shows a representative set of ex vivo susceptibility maps detailing anterior commissure region of both DEMY group and REMY group, with (a, c) and without (b, d) Gd contrast agent administration. The susceptibility value in DEMY group at AC region changed to −15.8 ± 4.9 ppb (with Gd) from - 4.1 ± 2.8 ppb (without Gd); the susceptibility value in REMY group at AC region changed to −30.9 ± 7.4 ppb (with Gd) from - 6.9 ± 3.4 ppb (without Gd).

Histology

Figure 10 shows representative brain slices of DEMY, REMY, and CTRL groups stained with Luxol Fast Blue (LFB) and Perl's Prussian Blue (PPB). There was a clear trend of increasing LFB contrast from DEMY group to REMY group in the CC, AC, CX, and EC area, while the contrast was strongest for CTRL group. On the contrary, the PPB contrast variation was little among these three groups. Enlarged images in CC and EC regions demonstrated 9 weeks recovery was not enough to return to the normal level, which was consistent with QSM findings (Fig. 3). Enlarged images in AAC and IAC demonstrated the intraregional demyelination variation in AC, CC, EC, and CX region.

Discussion

Cuprizone mouse model is a well-established demyelination model, and previous studies have shown MRI can detect WM lesions noninvasively (4,5,13). In this study, we imaged the whole brain of the cuprizone mouse both in vivo and ex vivo using different MRI techniques, including T2-weighted imaging, QSM, and DTI. The sensitivity to demyelination/remyelination process is strongly dependent on the quantitative parameters derived from different MRI modalities. It is interesting to notice that the demyelination was not only regionally different in different WM bundles, but also exhibited intraregional heterogeneity in the same WM bundle: the anterior part of AC exhibited more paramagnetic susceptibility than the posterior part of AC in the DEMY group. In comparison, little changes were observed in FA among DEMY, REMY, and CTRL group, while limited changes were exhibited in all DTI parameters between REMY mice and CTRL mice.

For multiple sclerosis, conventional T1 and T2 relaxation MRI techniques have demonstrated high detection sensitivity (25–27). From previous MRI and histology studies, significant changes started in normalized T2-weighted intensities of CC as early as 3 weeks post the start of cuprizone administration (4). Our results confirm and extend this investigation since dramatic T2-weighted image contrast variation was evident in CC area between the DEMY group and CTRL group in our long-term (up to 13 weeks) cuprizone administration. After 9 weeks recovery time, the REMY group showed similar but still visually lower T2-weighted contrast than age-matched CTRL mice. These data suggest that even 9 weeks recovery does not present complete normalization with respect to healthy age-matched controls, which may demonstrate the need for age-matched control mice in quantitative assessing the demyelination and remyelination process (5).

Previous reports have suggested that AD and RD can be used as noninvasive markers to probe the demyelination in the mouse corpus callosum in vivo (28,29). Song et al. found the extent of increased RD in cuprizone treated mouse brain and AD values of corpus callosum were not altered relative to non-treated mice (30). However, recently studies showed both AD and RD were significant higher in both the CC and EC of the cuprizone-fed mice when compared with controls (4). Note that interpreting changes of AD and RD on the basis of the underlying tissue microstructure should be accompanied by a thoroughly investigation of their mathematical and geometrical properties (31). Our results from DTI experiments demonstrated significant higher values of AD (17.5%) and RD (28.3%) in CC area between DEMY group and CTRL group. These data indicate that RD is more sensitive to the demyelination process than AD in cuprizone mice model.

FA value in CC was found to decrease after cuprizone treatment in both acute and chronic demyelination (4,28). Falangola et al. observed no significant FA variations between mice with 10 weeks cuprizone administration and control mice in rostral CC (0.26 vs 0.24), but significant decrease in middle CC (0.32 vs 0.27, $p < 0.001$) and caudal CC (0.46 vs 0.36, $p < 0.001$) (32). In our study, FA values also decreased about 6.8 % after 13 weeks cuprizone administration (0.44 vs 0.41). The difference may be caused by the different duration of cuprizone treatment and/or the different fixation process which could alter the ratio of intracellular and extracellular spaces, membrane permeability, and other physiological

variations (33,34). Overall, our results indicate that RD is a more sensitive and specific marker of demyelination than FA value (30).

Previous studies of shiverer mice and prenatal alcohol exposure models demonstrate that myelin is the dominant source of susceptibility contrast in WM (11,12,35). We observed a significant increase of susceptibility values in CC and AC regions in the cuprizone-fed mice compared to the CTRL mice, resulting in variation of susceptibility contrast between these WM regions and surrounding gray matter: reduction of contrast in vivo, and inversion of contrast ex vivo. These changes suggest that myelin is an important source of susceptibility contrast in brain parenchyma, which agrees with frequency contrast studies of mice models and studies in human neonates (36).

It is evident that the cuprizone-induced mice typically exhibit profound demyelination in the CC and cortex regions. Besides the regional demyelination variations of different WM tracts observed by multiparametric MRI measurements, the intraregional difference in CC and AC regions is also obvious using QSM. This regional heterogeneity demyelination suggested differences in the underlying pathophysiology, it may be essential in not only understanding the mechanisms involved in this model, but also in appropriately and effectively applying it to study human MS disease (6,7).

Almost complete demyelination in CC area is achieved by 4–6 weeks cuprizone treatment, this process is known as “acute demyelination” (37). The chronic demyelination is normally referred to prolonged administration of cuprizone. Many reports showed that withdrawal of the toxin resulted in spontaneous remyelination after acute demyelination (3). In this study, REMY group was treated by cuprizone for 4 weeks to mimic the acute demyelination, 9 weeks of recovery time were given to access the remyelination status. Since myelin is the main diamagnetic source in the WM regions, the significant susceptibility contrast variation in CC and AC areas between REMY group and DEMY group suggest a remarkable remyelination after 9 weeks of recovery time, this is also confirmed by the contrast change in T2-weighted and the histology results. The significantly higher susceptibility values of the REMY group than that of the CTRL mice again, imply the remyelination may not be fully completed even after 9 weeks of recovery time and the age-matched controls are in fact essential for cuprizone mice model study.

Postmortem MRI of tissue offers advantages over in vivo imaging in that it is not subject to motion artifacts and can be imaged with much higher spatial resolution, as prolonged scan times are not a limiting factor (29). The effect of tissue fixation on MRI parameters such as T2 and DTI parameters has been performed in fixed tissues and the results were used to infer the contrast expected in vivo MRI (38). Fixation can significantly change tissue microstructure and diffusion MR measurements and affect their capability to detect WM pathology. Recently, it has been reported that T2* and frequency contrast also change after tissue fixation (36). Both in vivo and ex vivo QSM results are sensitive to the demyelination/remyelination process, while the subtle variations in the intraregional WM tracts (CC, AC) were better detected by ex vivo scans.

Note that for fixed tissue in this study, Gd ions were administrated into the tissue to shorten T1 relaxation time and reduce the scan time. A previous study demonstrated white-gray matter contrast improves significantly as a function of gadolinium contrast agent in the tissue since WM appears increasing more diamagnetic relative to gray matter (39). The ex vivo susceptibility contrast was indeed enhanced by the Gd ion administration in our study. Consequently, this paramagnetic particle administration could also play an important role to the tissue susceptibility contrast.

The absolute susceptibility values measured ex vivo were influenced by the administration of Gd ions, however, the intraregional susceptibility contrast variation could be observed even without the use of Gd ions. It may suggest that, while the contrast may be elevated using Gd contrast agent, it does not alter the findings for both demyelination and remyelination process. Furthermore, the temperature difference between in vivo (37 ºC) and ex vivo (25 ºC) QSM scans could also contribute to the observed contrast changes (35). In general, the measured susceptibility value, even different between in vivo and ex vivo experiments, however, was demonstrated to be a sensitive biomarker for demyelination detection.

A limitation of the study is the relatively small sample size, larger sample size may help to improve our current results and extend our results to subtle variations in more brain regions. Second, we only compared the demyelination and remyelination process in one timing point, further studies in cuprizone mice model are also warranted to determine the time course of demyelination and remyelination using QSM method. Third, the T2, QSM, and DTI experiments are scanned with different spatial resolution, the effect of the partial volume effect is warranted in further investigated. It has been reported that WM bundles exhibit orientation-dependent magnetic susceptibility, the sensitivity of QSM to demyelination/remyelination is likely to be affected by the specimen orientation to the main magnetic field (9,40). In addition, QSM is sensitive to myelin and iron in the brain tissue, where tissue become more paramagnetic with iron deposit and demyelination (9,40). In the current study, the histology results only include myelin and iron (without distinguish the iron present in the myelin itself and the iron accumulated by active microglia) stains, additional sections with axonal and inflammation markers need to perform to validate with MRI findings.

In conclusion, we demonstrated that ex vivo QSM exhibited higher sensitivity to demyelination process of cuprizone exposure than DTI metrics. Significant regional and intraregional susceptibility contrast variation in major WM tracts of mouse brain was confirmed both in vivo and ex vivo resulting from cuprizone exposure. The demyelination and remyelination found in cortex, and external capsule demonstrated the complexity of the widely used cuprizone mouse mode. The significant abnormalities of magnetic susceptibility in major WM fibers are likely due to the extent of myelin depletion. Our data further indicates that magnetic susceptibility is sensitive to demyelination and remyelination process both in vivo and ex vivo MRI.

Supplementary Material

Refer to Web version on PubMed Central for supplementary material.

Acknowledgments

The authors thank Dr. G. Allan Johnson for access to the 7.0T and 9.4T scanners at Duke Center for In Vivo Microscopy, Dr. John Nouls and Gary Cofer for their technical assistance. This study was supported in part by the National Institutes of Health (NIH) through grants NIBIB P41 EB015897, and R01 MH096979 and by the National Multiple Sclerosis Society (RG4723).

List of abbreviations:

WM	white matter
CC	corpus callosum
AC	anterior commissure
HC	hippocampus commissure
QSM	quantitative susceptibility mapping
MS	multiple sclerosis
DTI	diffusion tensor imaging
DKI	diffusion kurtosis imaging
MTI	magnetization transfer imaging
AD	axial diffusivity
RD	radial diffusivity
MD	mean diffusivity
FA	fractional anisotropy
CTRL	control group
DEMY	demyelination group
REMY	remyelination group
CSF	cerebrospinal fluid
LFB	Luxol Fast Blue
PPB	Perl’s Prussian Blue
gCC	genu corpus callosum
iCC	body/isthmus corpus callosum
sCC	splenium corpus callosum
AAC	anterior part of anterior commissure
IAC	intermediate part of anterior commissure

PAC	posterior part of anterior commissure

References

1. Lucchinetti C, Brück W, Parisi J, Scheithauer B, Rodriguez M, Lassmann H. A quantitative analysis of oligodendrocytes in multiple sclerosis lesions. Brain 1999;122:2279–2295. [PubMed: 10581222]
2. Lucchinetti C, Bruck W, Parisi J, Scheithauer B, Rodriguez M, Lassman H. Heterogeneity of multiple sclerosis lesions: implications for the pathogenesis of demyelination. Ann Neurol 2000;47:707–717. [PubMed: 10852536]
3. Morell P, Barrett C, Mason J, et al. Gene expression in brain during cuprizone-induced demyelination and remyelination. Molecular and Cellular Neuroscience 1998;12:220–227. [PubMed: 9828087]
4. Thiessen JD, Zhang Y, Zhang H, et al. Quantitative MRI and ultrastructural examination of the cuprizone mouse model of demyelination. NMR Biomed 2013;26:1562–1581. [PubMed: 23943390]
5. Tagge I, O'Connor A, Chaudhary P, et al. Spatio-Temporal Patterns of Demyelination and Remyelination in the Cuprizone Mouse Model. Plos One 2016;11:e0152480. [PubMed: 27054832]
6. Guglielmetti C, Le Blon D, Santermans E, et al. Interleukin-13 immune gene therapy prevents CNS inflammation and demyelination via alternative activation of microglia and macrophages. Glia 2016;64:2181–2200. [PubMed: 27685637]
7. Guglielmetti C, Veraart J, Roelant E, et al. Diffusion kurtosis imaging probes cortical alterations and white matter pathology following cuprizone induced demyelination and spontaneous remyelination. Neuroimage 2016;125:363–377. [PubMed: 26525654]
8. Li W, Wu B, Liu C. Quantitative susceptibility mapping of human brain reflects spatial variation in tissue composition. Neuroimage 2011;55:1645–1656. [PubMed: 21224002]
9. Liu C Susceptibility tensor imaging. Magn Reson Med 2010;63:1471–1477. [PubMed: 20512849]
10. Li W, Liu C, Duong TQ, van Zijl PC, Li X. Susceptibility tensor imaging (STI) of the brain. NMR Biomed 2017;30:e3540.
11. Liu C, Li W, Johnson GA, Wu B. High-field (9.4 T) MRI of brain dysmyelination by quantitative mapping of magnetic susceptibility. Neuroimage 2011;56:930–938. [PubMed: 21320606]
12. Cao W, Li W, Han H, et al. Prenatal alcohol exposure reduces magnetic susceptibility contrast and anisotropy in the white matter of mouse brains. NeuroImage 2014;102:748–755. [PubMed: 25175539]
13. Turati L, Moscatelli M, Mastropietro A, et al. In vivo quantitative magnetization transfer imaging correlates with histology during de-and remyelination in cuprizone-treated mice. NMR in Biomedicine 2015;28:327–337. [PubMed: 25639498]
14. Ziser L, Meyer-Schell N, Kurniawan ND, et al. Utility of gradient recalled echo magnetic resonance imaging for the study of myelination in cuprizone mice treated with fingolimod. NMR Biomed 2018;31:e3877.
15. Sun SW, Neil JJ, Song SK. Relative indices of water diffusion anisotropy are equivalent in live and formalin-fixed mouse brains. Magnetic resonance in medicine 2003;50:743–748. [PubMed: 14523960]
16. Li W, Wang N, Yu F, et al. A method for estimating and removing streaking artifacts in quantitative susceptibility mapping. Neuroimage 2015;108:111–122. [PubMed: 25536496]
17. Schweser F, Deistung A, Lehr BW, Reichenbach JR. Quantitative imaging of intrinsic magnetic tissue properties using MRI signal phase: an approach to in vivo brain iron metabolism? Neuroimage 2011;54:2789–2807. [PubMed: 21040794]
18. Wang N, Cofer G, Anderson RJ, Qi Y, Liu C, Johnson GA. Accelerating quantitative susceptibility imaging acquisition using compressed sensing. Phys Med Biol 2018;63:245002. [PubMed: 30524114]
19. Basser PJ, Pierpaoli C. Microstructural and physiological features of tissues elucidated by quantitative-diffusion-tensor MRI. J Magn Reson B 1996;111:209–219. [PubMed: 8661285]
20. Wang N, Anderson RJ, Badea A, et al. Whole mouse brain structural connectomics using magnetic resonance histology. Brain Structure & Function 2018;223:4323–4335. [PubMed: 30225830]

21. Wang N, Mirando AJ, Cofer G, Qi Y, Hilton MJ, Johnson GA. Diffusion tractography of the rat knee at microscopic resolution. Magn Reson Med 2019;81:3775–3786. [PubMed: 30671998]
22. Johnson GA, Badea A, Brandenburg J, et al. Waxholm Space: An image-based reference for coordinating mouse brain research. Neuroimage 2010;53:365–372. [PubMed: 20600960]
23. Yushkevich PA, Piven J, Hazlett HC, et al. User-guided 3D active contour segmentation of anatomical structures: Significantly improved efficiency and reliability. Neuroimage 2006;31:1116–1128. [PubMed: 16545965]
24. Winkler AM, Ridgway GR, Webster MA, Smith SM, Nichols TE. Permutation inference for the general linear model. Neuroimage 2014;92:381–397. [PubMed: 24530839]
25. van Walderveen MAA, Kamphorst W, Scheltens P, et al. Histopathologic correlate of hypointense lesions on T1-weighted spin-echo MRI in multiple sclerosis. Neurology 1998;50:1282–1288. [PubMed: 9595975]
26. Kolind SH, Laule C, Vavasour IM, et al. Complementary information from multi-exponential T2 relaxation and diffusion tensor imaging reveals differences between multiple sclerosis lesions. Neuroimage 2008;40:77–85. [PubMed: 18226549]
27. Petiet A, Aigrot M-S, Stankoff B. Gray and white matter demyelination and remyelination detected with multimodal quantitative MRI analysis at 11.7 T in a chronic mouse model of multiple sclerosis. Frontiers in neuroscience 2016;10:491. [PubMed: 27833528]
28. Sun SW, Liang HF, Trinkaus K, Cross AH, Armstrong RC, Song SK. Noninvasive detection of cuprizone induced axonal damage and demyelination in the mouse corpus callosum. Magnetic Resonance in Medicine 2006;55:302–308. [PubMed: 16408263]
29. Zhang J, Jones MV, McMahon MT, Mori S, Calabresi PA. In vivo and ex vivo diffusion tensor imaging of cuprizone-induced demyelination in the mouse corpus callosum. Magnetic resonance in medicine 2012;67:750–759. [PubMed: 21656567]
30. Song S-K, Yoshino J, Le TQ, et al. Demyelination increases radial diffusivity in corpus callosum of mouse brain. NeuroImage 2005;26:132–140. [PubMed: 15862213]
31. Wheeler-Kingshott CA, Cercignani M. About “axial” and “radial” diffusivities. Magnetic Resonance in Medicine: An Official Journal of the International Society for Magnetic Resonance in Medicine 2009;61:1255–1260.
32. Falangola MF, Guilfoyle DN, Tabesh A, et al. Histological correlation of diffusional kurtosis and white matter modeling metrics in cuprizone-induced corpus callosum demyelination. NMR in Biomedicine 2014;27:948–957. [PubMed: 24890981]
33. Beaulieu C The basis of anisotropic water diffusion in the nervous system–a technical review. NMR in Biomedicine 2002;15:435–455. [PubMed: 12489094]
34. Neil J, Miller J, Mukherjee P, Hüppi PS. Diffusion tensor imaging of normal and injured developing human brain-a technical review. NMR in Biomedicine 2002;15:543–552. [PubMed: 12489100]
35. Lee J, Shmueli K, Kang B-T, et al. The contribution of myelin to magnetic susceptibility-weighted contrasts in high-field MRI of the brain. NeuroImage 2012;59:3967–3975. [PubMed: 22056461]
36. Lodygensky GA, Marques JP, Maddage R, et al. In vivo assessment of myelination by phase imaging at high magnetic field. NeuroImage 2012;59:1979–1987. [PubMed: 21985911]
37. Matsushima GK, Morell P. The neurotoxicant, cuprizone, as a model to study demyelination and remyelination in the central nervous system. Brain Pathology 2001;11:107–116. [PubMed: 11145196]
38. Dawe RJ, Bennett DA, Schneider JA, Vasireddi SK, Arfanakis K. Postmortem MRI of human brain hemispheres: T2 relaxation times during formaldehyde fixation. Magnetic resonance in medicine 2009;61:810–818. [PubMed: 19189294]
39. Dibb R, Li W, Cofer G, Liu C. Microstructural origins of gadolinium-enhanced susceptibility contrast and anisotropy. Magnetic resonance in medicine 2014;72:1702–1711. [PubMed: 24443202]
40. Wharton S, Bowtell R. Fiber orientation-dependent white matter contrast in gradient echo MRI. P Natl Acad Sci USA 2012;109:18559–18564.

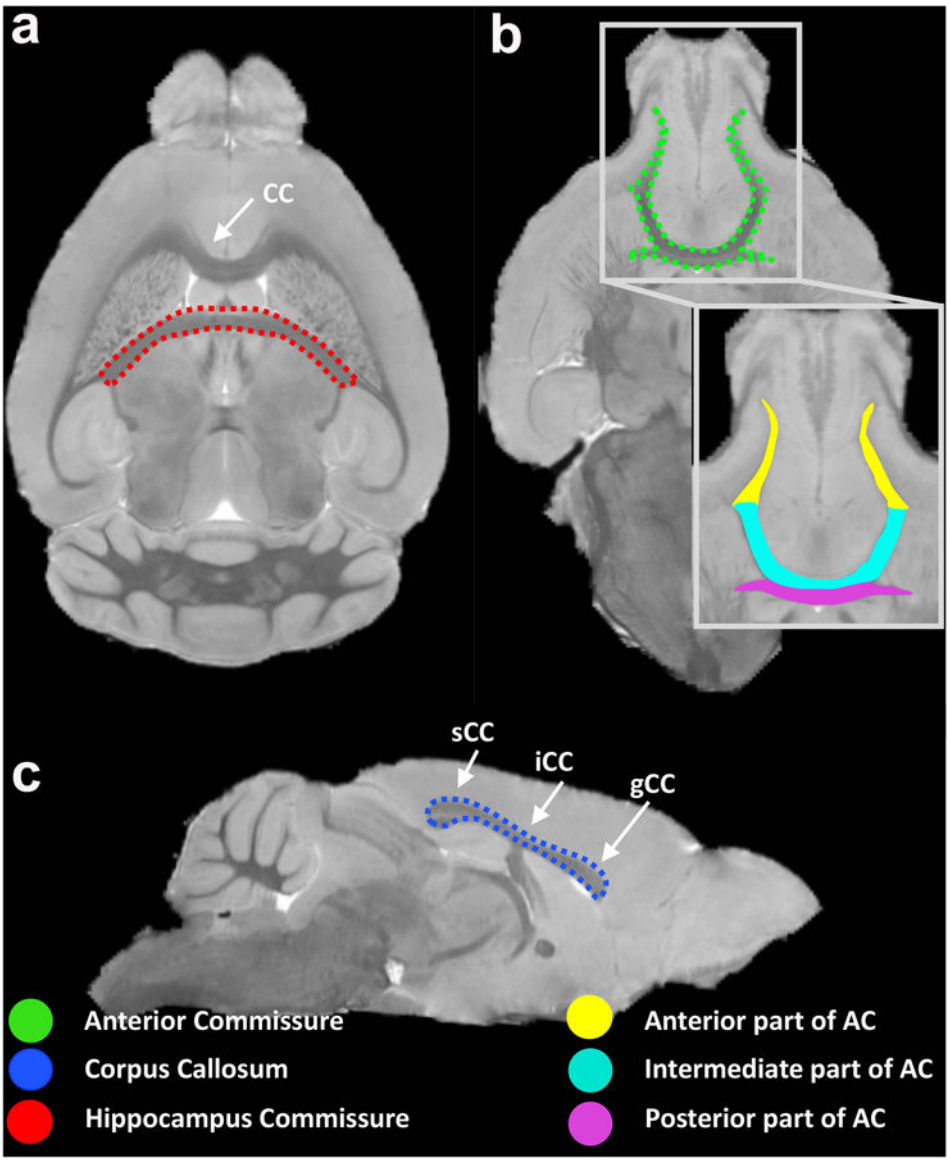

FIGURE 1.

Delineation of anterior commissure (green), corpus callosum (blue), and hippocampus commissure (red) of one mouse brain in native space, the genu (gCC), body/isthmus (iCC), and splenium (sCC) were pointed by white arrows. The anterior commissure was further subdivided to 3 parts: anterior part, intermediate part, and posterior part.

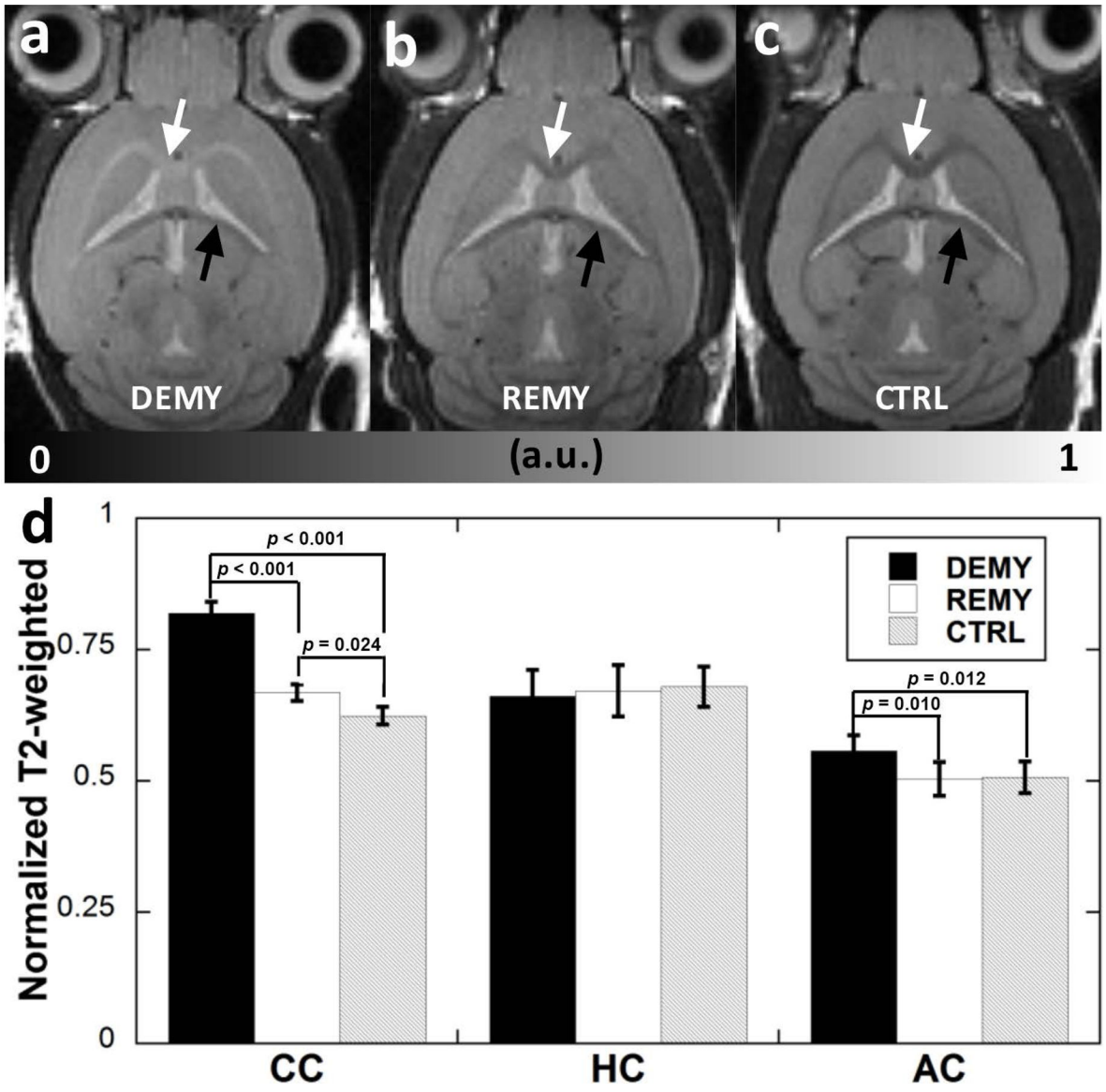

FIGURE 2.

Normalized T2-weighted (a-c) images of DEMY (a), REMY (b), and CTRL (c) mice. Compared to CTRL and REMY mice, signal inversion in the T2-weighted (white arrows) of cuprizone administration mice are obvious in CC region. Normalized T2-weighted images illustrated significant differences in signal intensity among three groups in the CC (d) and AC areas, while no significant differences in HC area (black arrows).

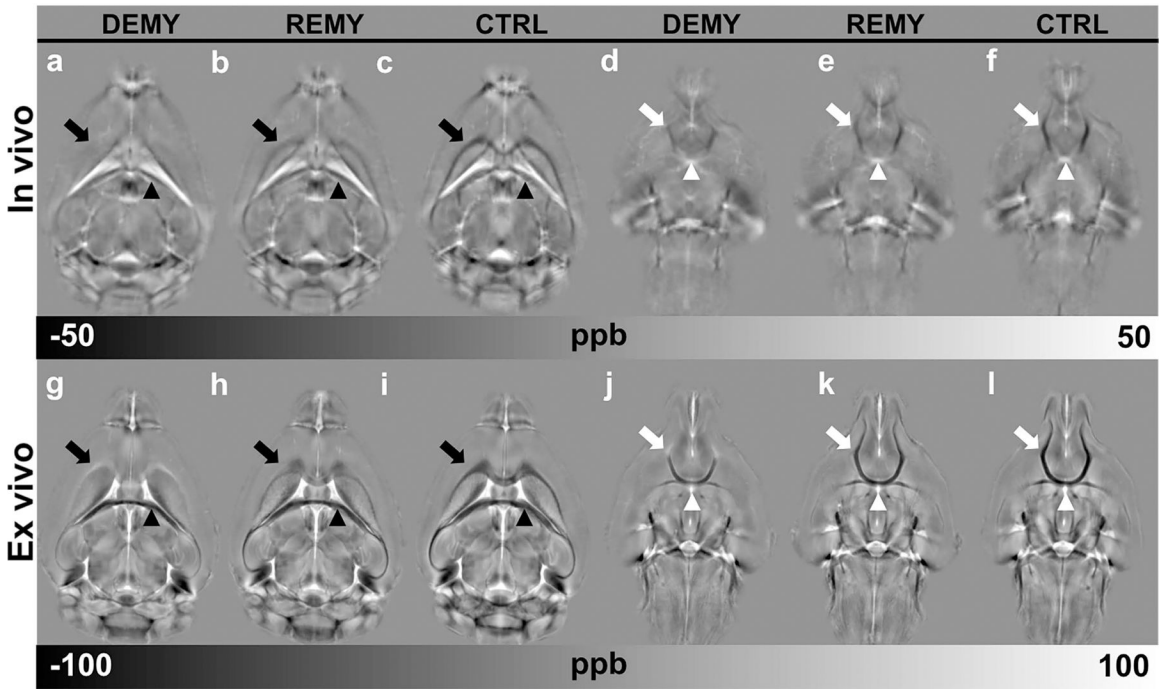

FIGURE 3.

A representative set of in vivo (a-f) and ex vivo (g-i) susceptibility maps for the DEMY, REMY, and CTRL groups. White matter bundles exhibited strongest diamagnetic susceptibility in CTRL group and least diamagnetic susceptibility in DEMY group except the HC region (black arrowheads). The susceptibility contrast of REMY group between CC (black arrows) and surrounding tissue is still not as strong as that of CTRL mice even after 9 weeks recovery time. DEMY group had clearly inhomogeneous susceptibility contrast in AC region (white arrows). Compared to the ex vivo susceptibility mapping, the posterior part of AC in vivo is barely visible due to the strong paramagnetic source in that area (white arrowheads).

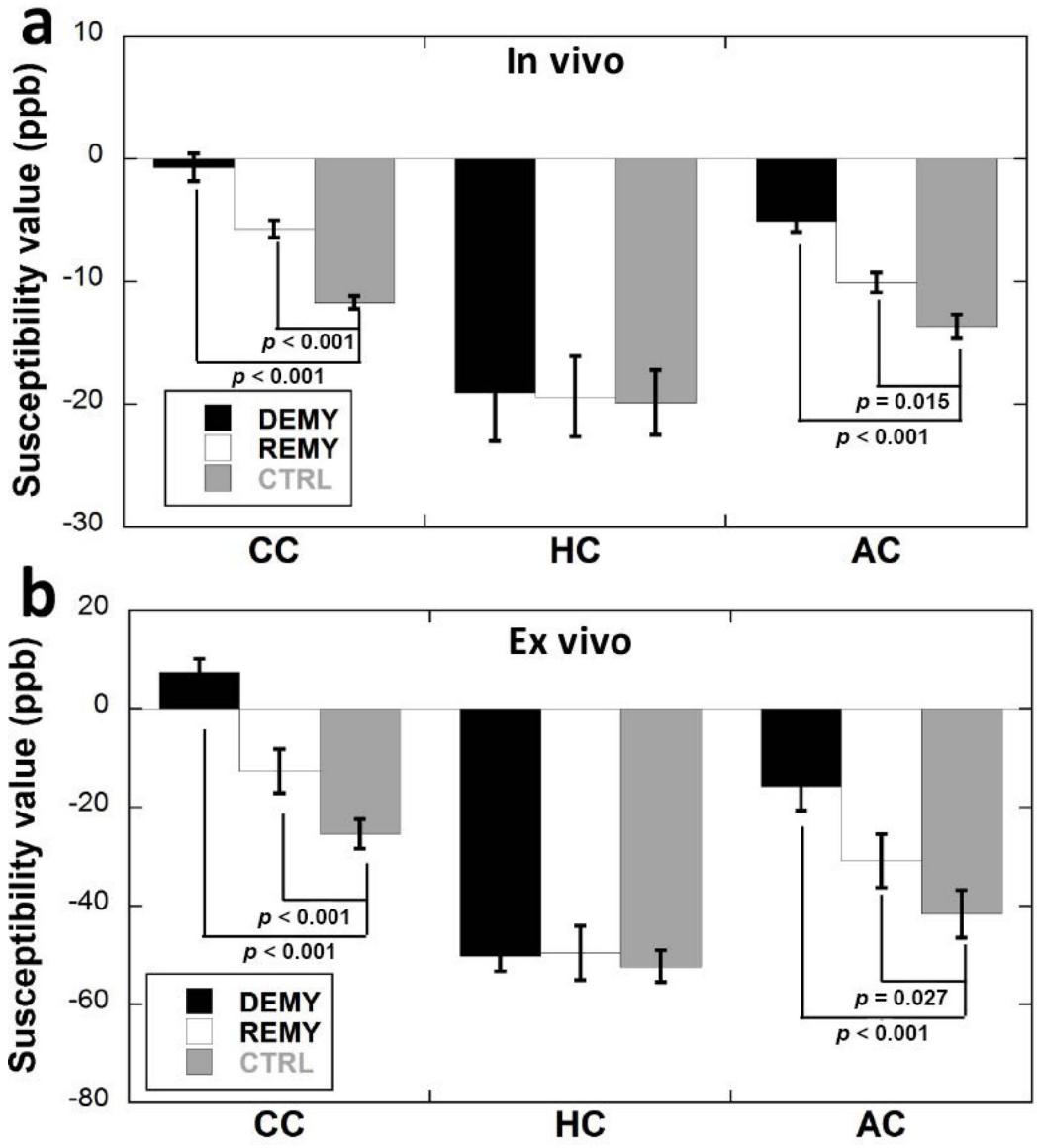

FIGURE 4.

Statistical comparison of susceptibility values in three ROIs among the DEMY, REMY, and CTRL group (n = 5). Significant differences between DEMY and CTRL group, between REMY group and CTRL group were observed in CC and AC regions both in vivo (a) and ex vivo (b). No significant difference was observed among these three groups in HC area.

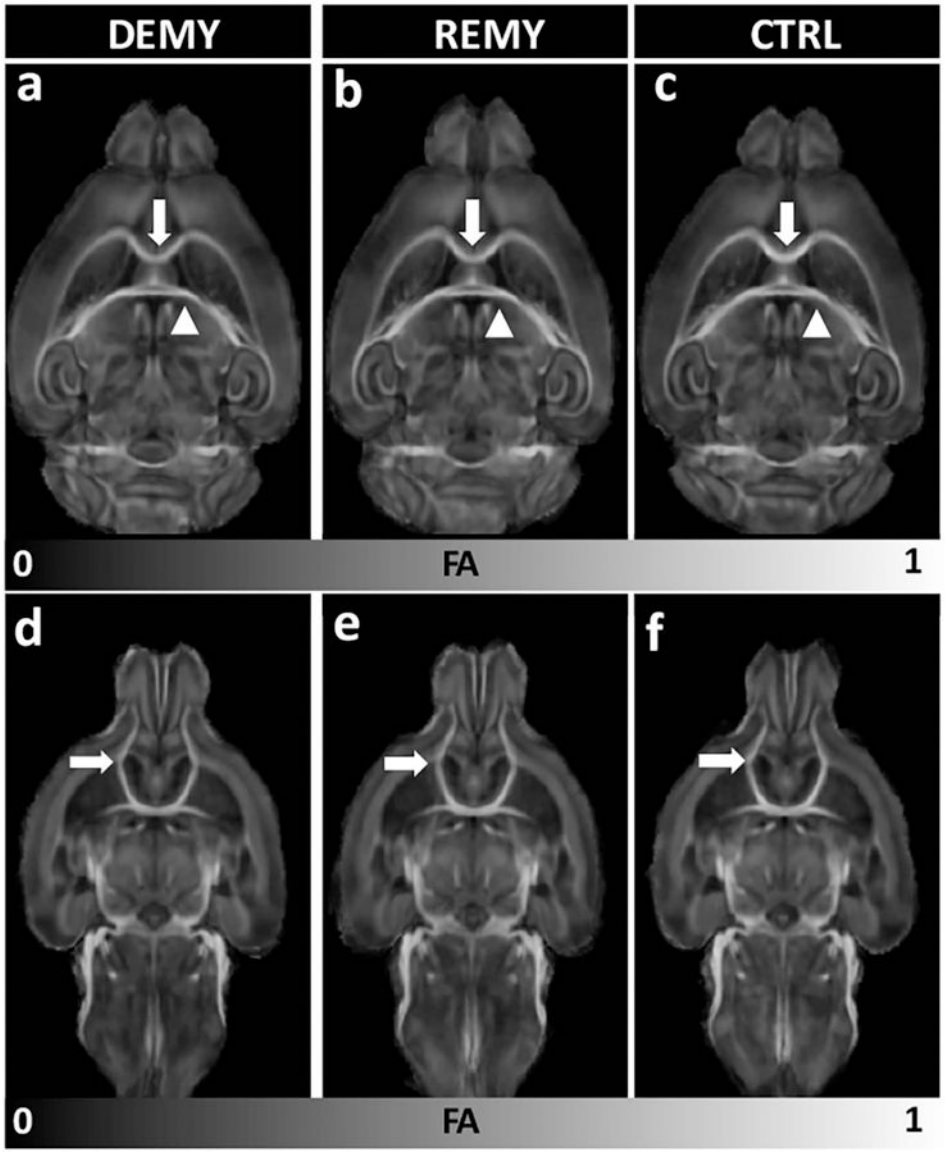

FIGURE 5.

Comparison of FA maps in two representative slices among DEMY (a, d), REMY (b, e), and CTRL (c, f) group. The differences in the CC (white arrows in a-c), HC (arrow heads), and AC (white arrows in d-f) are visually less obvious compared to QSM in Fig 4.

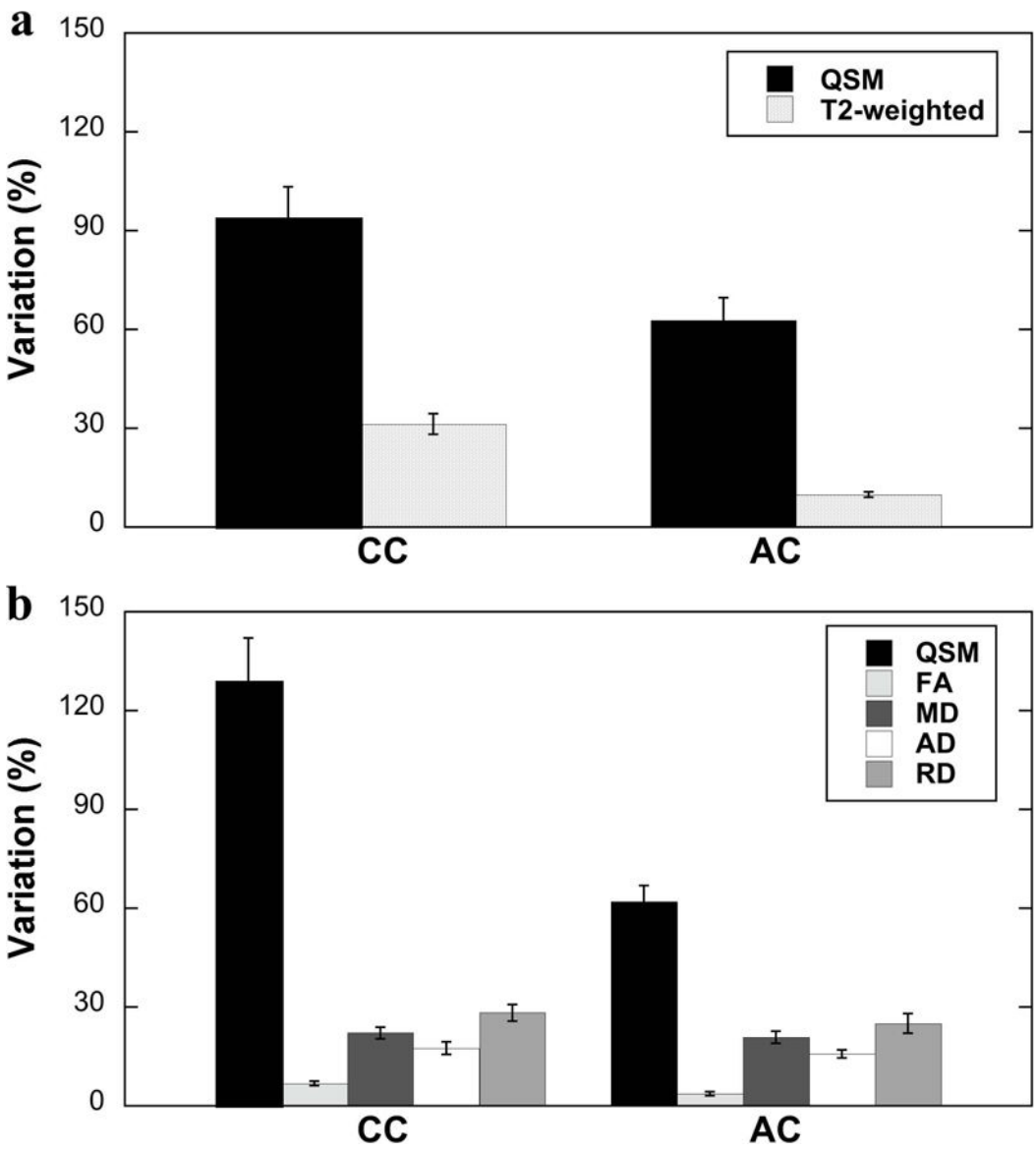

FIGURE 6.

Sensitivity of MRI parameters to demyelination process of cuprizone administration. Susceptibility values showed higher variations than DTI metrics for ex vivo studies.

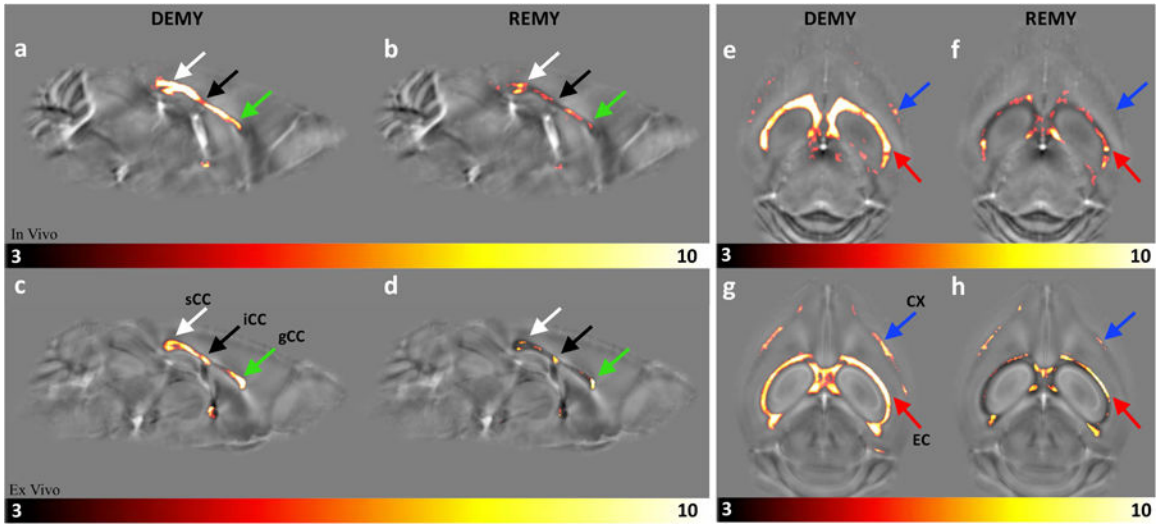

FIGURE 7.

In vivo and ex vivo voxel-based analysis of susceptibility values in corpus callosum (CC), external capsule (EC), and cortex (CX) regions. CC structure was separated into genu (gCC), body/isthmus (iCC), and splenium (sCC) regions, respectively. Compared to CTRL group, the susceptibility values of DEMY group increase significantly in CC, EC (red arrows), and CX (blue arrows) areas. The variations are largely eliminated in REMY group, however, the significant susceptibility difference can still be resolved in these regions between REMY and CTRL. Note the CX susceptibility variation is shown in ex vivo results (h), but it's not shown in in vivo results. The color scale indicates t value of contrast with the significant level was set up as $p = 0.05$ with Family-wise (FWE) correction.

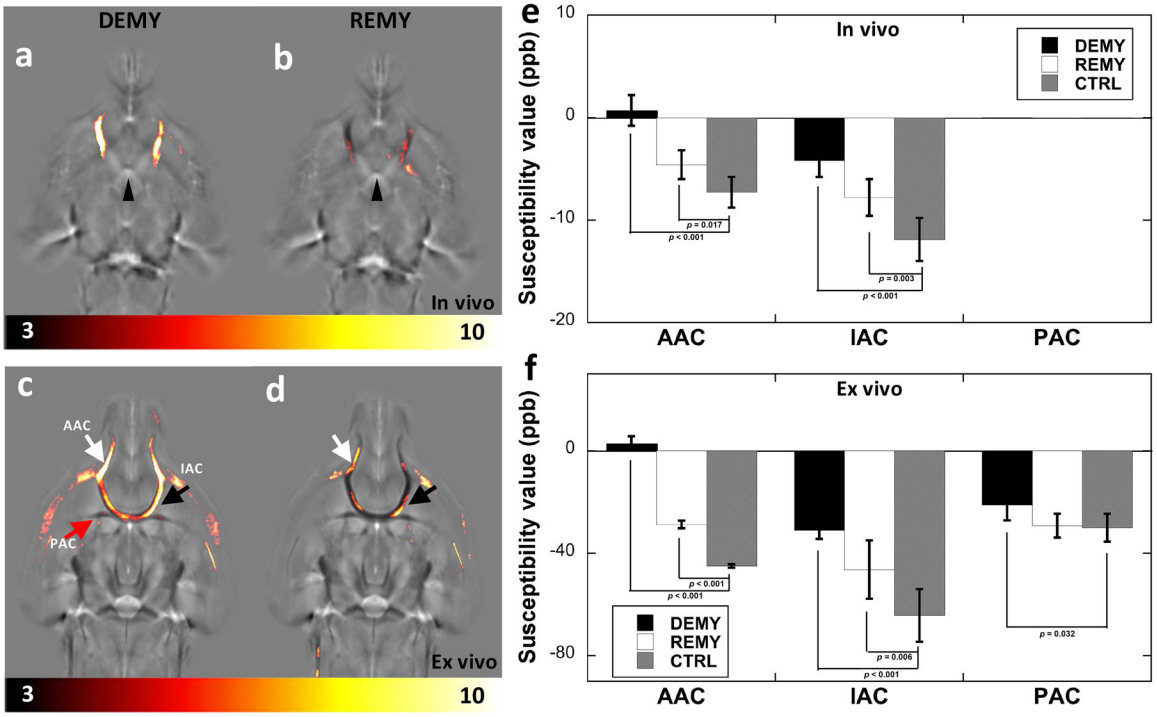

FIGURE 8.

In vivo and ex vivo regional susceptibility heterogeneity in AC region. Anterior commissure was divided into three zones: anterior part of AC (AAC), intermediate part of AC (IAC), and posterior part of AC (PAC). Susceptibility value of DEMY group was always lower than that of CTRL group. Susceptibility value of REMY group was always lower than that of CTRL group in AAC region, while there was no significant difference at PAC region. The color scale indicates t value of contrast with the significant level was set up as p = 0.05 with Family-wise (FWE) correction.

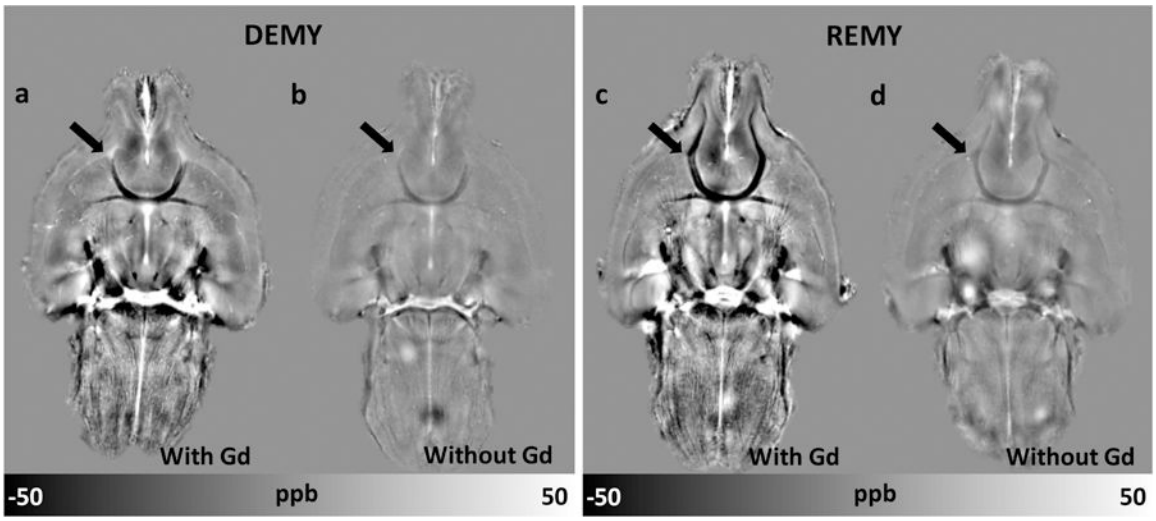

FIGURE 9.

A representative set of susceptibility maps detailing anterior commissure region (black arrows) of both DEMY and REMY mice, with (a, c) and without (b, d) contrast agent administration. White-gray matter susceptibility contrast is largely enhanced after Gd administration. However, the susceptibility variation shows similar change regardless of the contrast agent.

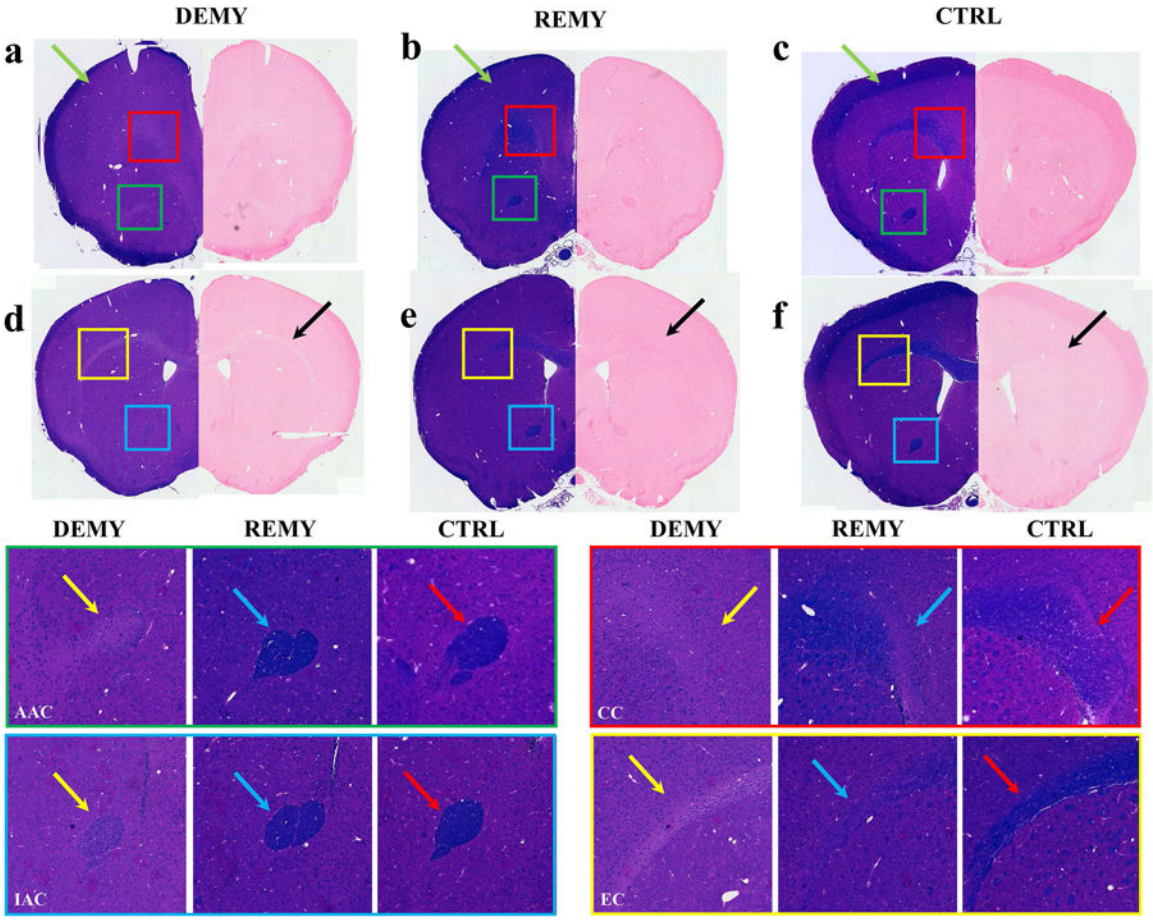

FIGURE 10.

Examples of histological slices among CTRL, DEMY, and REMY group: LFB stained slices under light microscopy (left panels in a-f) and corresponding PPB contrast (right panels in a-f). Enlarged images in CC, CX and EC regions demonstrate 9 weeks recovery is not enough to return to the normal level. Enlarged images in AAC and IAC demonstrated the intraregional demyelination variation in AC region.

Table 1

In vivo and ex vivo susceptibility values (ppb; mean ± SD) of brain regions in DEMY, REMY, and CTRL group.

	Groups	CC	HC	AC
In-Vivo	DEMY	−0.7±1.1	−19.1±3.9[a]	−5.1±0.9
	REMY	−5.7±0.7	−19.3±3.3[a]	−10.1±0.8
	CTRL	−11.7±0.5	−19.8±2.6[a]	−13.7±1.0
Ex-Vivo	DEMY	7.4±2.8	−50.1±3.1[b]	−15.8±4.9
	REMY	−12.7±4.4	−49.6±5.5[b]	−30.9±7.4
	CTRL	−25.4±3.0	−52.3±3.2[b]	−41.6±4.9

[a] These three sets of the in vivo susceptibility values (DEMY, REMY, and CTRL) have no significant difference ($p > 0.05$).

[b] These three sets of the ex vivo susceptibility values (DEMY, REMY, and CTRL) have no significant difference ($p > 0.05$).

Table 2

In vivo and ex vivo susceptibility values (ppb; mean ± SD) of CC and AC sub-regions in DEMY, REMY, and CTRL group.

		CC			AC		
	Groups	**MCC**	**ICC**	**LCC**	**AAC**	**IAC**	**PAC**
In Vivo	**DEMY**	5.0±1.7	−2.2±1.6	−1.5±0.9	1.7±1.5	−6.2±2.6	-
	REMY	−1.7±1.8	−11.1±1.6	−6.3±0.6	−4.6±2.1	−7.8±2.8	-
	CTRL	−11.2±2.4	−13.8±2.3	−8.1±1.1	−7.3±1.5	−11.9±3.1	-
Ex Vivo	**DEMY**	19.1±6.0	6.9±3.4	10.3±3.5	2.9±2.8	−31.1±3.4	−21.1±5.9
	REMY	−10.4±3.8	−19.6±6.6	−15.0±2.9	−28.7±1.5	−46.4±11.4	−29.3±4.7[a]
	CTRL	−22.6±3.1	−28.9±2.9	−23.2±4.0	−44.9±0.7	−64.3±10.3	−30.0±5.4[a]

[a] These two sets of the susceptibility values (REMY and CTRL) have no significant difference ($p > 0.05$).

[b] In vivo PAC values are not reported here since the PAC area could barely be differentiated probably due to the strong susceptibility source below the PAC area.

Table 3

Ex vivo FA, MD, AD, RD values (ppb; mean ± SD) of brain regions in DEMY, REMY, and CTRL group.

	FA			MD			AD			RD		
	CC	**HC**	**AC**	**CC**	**HC**	**AC**	**CC**	**HC**	**AC**	**CC**	**HC**	**AC**
DEMY	0.41±0.06	0.52±0.03	0.48±0.04	0.33±0.06*	0.32±0.03	0.29±0.02*	0.48±0.03*	0.49±0.05	0.44±0.04*	0.27±0.02*	0.23±0.02	0.20±0.02*
REMY	0.42±0.07	0.53±0.04	0.49±0.04	0.28±0.03	0.32±0.04	0.25±0.03	0.41±0.04	0.48±0.04	0.39±0.03	0.22±0.03	0.22±0.03	0.17±0.02
CTRL	0.44±0.05	0.54±0.05	0.51±0.05	0.27±0.03	0.30±0.04	0.24±0.03	0.41±0.03	0.47±0.05	0.38±0.04	0.21±0.02	0.21±0.03	0.16±0.03

*There is a significant difference between the DEMY group and CTRL group ($p < 0.05$).